Decisive influence of colloidal suspension conductivity during electrophoretic impregnation of porous anodic film supported on 1050 aluminium substrate

Benoit Fori, Pierre-Louis Taberna, Laurent Arurault, Jean-Pierre Bonino

Decisive influence of colloidal suspension conductivity during electrophoretic impregnation of porous anodic film supported on 1050 aluminium substrate

B. Fori [a], P.L. Taberna [b,*], L. Arurault [b], J.P. Bonino [b]

[a] Mecaprotec Industries, 34 Boulevard Joffrery, 31605 Muret Cedex, France
[b] Université de Toulouse, CIRIMAT UPS-CNRS, 118 route de Narbonne, 31062 Toulouse Cedex 9, France

A B S T R A C T

The present paper studies the influence of suspension conductivity on the electrophoretic deposition (EPD) of nanoparticles inside a porous anodic aluminium oxide film. It is shown that an increase in the suspension's conductivity enhances impregnation of the anodic film by the nanoparticles. Two mechanisms are seen to promote the migration of particles into the pores. Indeed an increase in the suspension conductivity leads on the one hand to a strengthening of the electric field in the anodic film and on the other hand to a thinning of the electric double layer on the pore walls. The results of our study confirm that colloidal suspension conductivity is a key parameter governing the electrophoretic impregnation depth.

Keywords:
Suspension conductivity
Aluminium alloy
Supported anodic film
Electrophoretic deposition

1. Introduction

Electrophoretic deposition (EPD) is a process allowing coatings to be prepared from colloidal dispersions. This method can be applied to a wide variety of materials including oxide particles [1], metallic particles [2], carbon nanotubes [3] and polymer particles [4]. It produces homogeneous deposits even on complex shaped substrates [5]. EPD has many additional advantages including its low cost, rapidity and easy implementation [6]. The quality of such electrophoretic deposits depends on many factors such as the voltage applied, the zeta potential, the concentration of solids in suspension and the conductivity of the substrate [6].

As has been previously demonstrated, suspension conductivity is also decisive in obtaining uniform EPD coating. Thus Stappers et al. [7] showed that uniform coatings were generated on flat surfaces using high-conductivity suspensions while low-conductivity suspensions resulted in non-uniform deposits. Nevertheless, a trade-off has to be found between high suspension stability when using low conductivity, and a high particle rate deposition for high conductivity [8]. Generally, finding the optimal solution depends on the surface chemical function of the particles [9], the solvent used [10] and additives such as surfactants [8].

Over the last 10 years, EPD has increasingly been used on highly porous substrates [11]. However, with the exception of Kamada et al. [12] and our team [13], EPD in anodic films still supported on aluminium alloy has not so far been extensively studied. Indeed, all previous studies [11] focused on the preparation of oxide nanorods and nanotubes by EPD using an anodic alumina membrane (AAM) as a template, secured to a metal foil. This technique involves using EPD to fill pores in the membrane and then removing the template membrane. The resulting materials offer a significantly larger surface area than that of flat films or bulk material, and thus find varied applications in nanotechnologies (sensors, batteries, SOFCs, etc.).

Limmer et al. [14] showed that zeta potential drives the migration and deposition of nanoparticles into AAM pores. When particles have a charge with opposite sign to that of the template, deposition results, preferably on the pore walls, where the electrostatic attraction between particles and the pore walls proves stronger than the applied electric field. It also emerged that voltage levels could affect the quality of electrophoretic deposits. When the voltage is too high, the velocity of the particles in the bulk solution also increases and the surface diffusion of particles into deposit defects (e.g., kinks, steps and holes) is correspondingly impaired, leading to the formation of a highly porous deposit [14]. However, to the best of our knowledge, the influence of the suspension conductivity has not been evaluated.

The objective of the present work is to investigate the role of the suspension conductivity on the EPD of silica nanoparticles in pores of an anodic film supported on an aluminium alloy. To this purpose, current/voltage measurements were obtained during EPD and FEG-SEM characterisations were performed on the resulting composite material, i.e., the anodic film with SiO_2 particles.

* Corresponding author.
E-mail address: taberna@chimie.ups-tlse.fr (P.L. Taberna).

http://dx.doi.org/10.1016/j.jcis.2013.08.011

2. Experimental set-up

2.1. Preparation of the standard anodic film

To facilitate the penetration of particles inside the pores, the porosity of the anodic films has to exhibit low tortuosity and pore diameters larger than those of the silica nanoparticles (i.e., 15 nm) [13]. 1050A aluminium alloy (chemical composition in per cent weight: 99.5% Al, <0.40% Fe, <0.25% Si and <0.05% Cu) was used as a substrate to obtain linear pores perpendicular to the initial metal surface. Since large pores (average pore diameter >100 nm) are required, a phosphoric acid based electrolyte was chosen as the anodising bath.

Firstly, the alloy sheet (20 mm × 20 mm × 1 mm) was degreased using ethanol. Secondly, the sample was etched in an NaOH aqueous solution (0.5 g L^{-1}) at 40 °C for 5 min and then neutralised in HNO_3 (25% vol) at room temperature for 2 min; the water used to make these solutions showed resistivity of 10 kΩ cm^{-1}. Thirdly, the aluminium sheet was used as an anode and a lead plate (2 × 40 × 40 mm) as a counter-electrode (i.e., here the cathode) in the electrochemical cell. The anodising process was run for 29 min in galvanostatic mode (TDK-Lambda GEN 300-5) using a current density of 1.5 A dm^2. The temperature was set to 25 °C. The samples were rinsed in deionised water (10 kΩ cm^{-1}) immediately following each step. Finally, the standard anodic film typically showed a pore diameter of 130 ± 10 nm, film thickness of 10 ± 1 μm and barrier layer thickness of 130 ± 5 nm [13].

2.2. Electrophoretic impregnation

A commercial colloidal suspension of silica nanoparticles (15 nm) in isopropyl alcohol (ABCR, Germany) was used. This suspension was diluted with isopropyl alcohol (Carlo Erba, Italy) to obtain a concentration of about 15 g L^{-1} and then vigorously stirred. Functionalisation of silica was performed in accordance with the procedure developed by Cousinié et al. [15]. 3 mL of aminopropyltrimethoxysilane (APTMS) was added dropwise to 100 mL of the diluted suspension. The mixture was then vigorously stirred for 3 days and then diluted 100 times with isopropyl alcohol, leading to a concentration of about 0.15 g L^{-1}. 1–15 mL of an I_2-acetone mixture (6 g L^{-1}) was added to the as-prepared suspension to modify its conductivity. In order to perform electrophoretic deposition, anodised aluminium was set as the cathode, while lead foil was used as the anode. A voltage of 600 V was applied (i.e., an electric field of 200 V cm^{-1}) for 5 min. The substrate was dried at ambient temperature after the experiment [13].

2.3. Characterisations

A Field Emission Gun Scanning Electron Microscope (FEG-SEM, JEOL JSM 6700F) was used to observe the microstructure of the coatings. The average impregnation depth was measured on the FEG-SEM cross-sectional views using the ImageJ software. Meanwhile, a MALVERN NANOSIZER ZS90 was used for zeta potential measurements. Conductivity was measured using a SympHony SB70D conductivity meter (VWR, France).

2.4. Current/voltage measurements

An ammeter was used to measure changes in current intensity as they occurred during EPD. Also, in order to evaluate the distribution of the electric field in the electrophoretic cell, a wire of 1050A aluminium alloy was located at 3 mm from the anodic film to act as a voltage probe. The voltage was measured with a voltmeter connected between this probe and the cathode, with values being recorded at sampling times of 1 s.

3. Results and discussion

3.1. Relation between impregnation depth and electrolyte conductivity

To modify the suspension conductivity, an I_2/acetone mixture was used. Conductivity increases with I_2 concentration as shown in Fig. 1. This increase is probably mainly due to the formation CH_3-CH_2ICOH^+ species that are created by reactions between I_2 and acetone [16]:

$$(CH_3)_2CO + I_2 \leftrightarrow (CH_3)_2CO^+I_2^- \quad (1)$$

$$(CH_3)_2CO^+I_2^- \rightarrow CH_3CH_2ICOH^+ + I^- \quad (2)$$

The zeta potential, which is initially negative and equal to −25 mV, first increases with the I_2 concentration and becomes positive. This phenomenon is due to $CH_3CH_2ICOH^+$ species that are adsorbed onto particle surface leading to zeta potential switching from negative to positive [16]. Beyond 50 mg L^{-1} of I_2, zeta potential then stabilises at about +25 mV. In these experimental conditions, at higher concentrations (>50 mg L^{-1}), repulsive interactions between ions are preponderant in comparison with attractive interactions between ions and particles. No more ion can go inside the double layer. Therefore, the zeta potential increases no further, remaining constant as the I_2 concentration increases.

According the Hückel equation (5), electrophoretic mobility μ (m^2 s^{-1} V^{-1}) is directly proportional to the zeta potential [6]:

$$\mu = \frac{2\zeta\varepsilon_0\varepsilon_r}{3\pi\eta} \quad (3)$$

with ζ the zeta potential (V), ε_r relative permittivity of the fluid, ε_0 the vacuum permittivity (8.845 × 10^{-12} F m^{-1}) and η the dynamic viscosity (Pa s). In order to minimise the influence of the zeta potential in this study, the I_2 concentration was adjusted to between 50 mg L^{-1} and 300 mg L^{-1} since, in this concentration range, the zeta potential can be considered to be constant. Furthermore, its positive value indicates that particles should migrate towards the cathode (i.e., the negative electrode) during electrophoretic migration. This should avoid over-oxidation of the aluminium foil, which can occur if it is used as an anode during EPD, thus leading to a change in the anodic film microstructure [17]. It is also known that the barrier layer is poorly conductive. By applying cathodic polari-

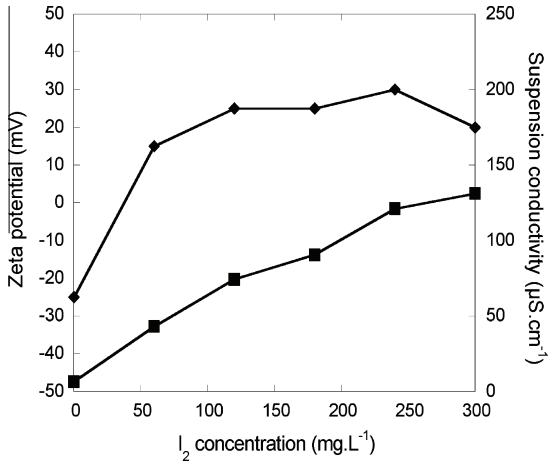

Fig. 1. Zeta potential (♦) and suspension conductivity (■) versus the I_2 concentration.

sation, the barrier layer of the anodic film behaves like an n-type semi-conductor, so the current can pass through it [18]. This should improve the efficiency of the impregnation.

Electrophoretic impregnations of the standard anodic film lasting 5 min were performed using an electric field of 200 V cm^{-1} (Fig. 2), for different suspension conductivities. FEG-SEM views reveal that low suspension conductivity (40 μS cm^{-1}) leads to the formation of a deposit only at the surface of the anodic film (nothing inside the pores), whereas the pores become completely filled by nanoparticles for higher suspension conductivity levels (120 μS cm^{-1}). The average impregnation depth of the particles was measured as a function of the conductivity (Fig. 3). For conductivities lower than 40 μS cm^{-1}, particles deposited only at the anodic film surface, indicating that particles migrated towards the anodic film but could not penetrate the pores. This is certainly due to charge interactions between the particles and the pore walls. However, impregnation proved possible and gradually increased for conductivities over 40 μS cm^{-1}. Pores were completely filled when the suspension conductivity was equal to 120 μS cm^{-1}. These results suggest that an increase in conductivity improves the migration of particles into the pores and accelerates the impregnation rate of the film.

3.2. Focus on the electric field through the anodic film

The potential difference between the cathode and the probe located at 3 mm from the anodic film was measured during the EPD. This difference was plotted as a function of the duration, for each suspension conductivity (Fig. 4). For conductivities lower than 120 μS cm^{-1}, the potential difference first decreases and then increases during deposition. The decrease suggests that the potential gradient in the anodic film decreases. This can be attributed to the dielectric breakdown of the film that can occur for a high applied voltage. However, the increase that ensues can certainly be explained by the resistance of the particles deposited in the pores. When conductivity is equal to 120 μS cm^{-1}, no decrease is observed but rather an increase can be noted. This can be ascribed to the strong increase in resistance relative to the presence of particles (because of a more compact deposit is formed according to [7]) in the anodic film that completely counters the decrease due to the dielectric breakdown of the film.

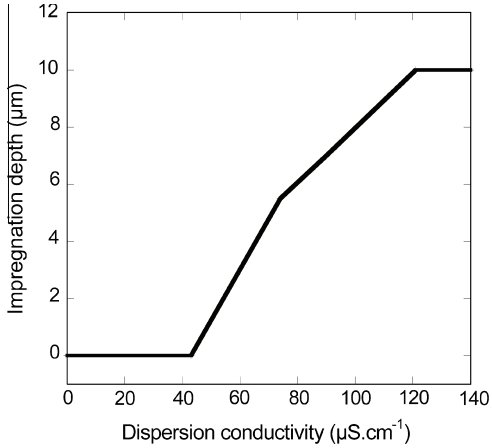

Fig. 3. Impregnation depth versus suspension conductivity (200 V cm^{-1}, 5 min).

The value of the potential difference between the probe and the cathode increases with the suspension conductivity, meaning that the electric field through the anodic film increases. On the one hand, the increase in the suspension's conductivity leads to a decrease in its resistance. This reduction minimises the Ohmic losses in the suspension, leading in turn to a decrease in the electric field in the suspension. On the other hand, the concomitant electric field through the anodic film inevitably increases. When conductivity is equal to 40 μS cm^{-1}, the potential gradient in the pores is too weak and particle agglomeration occurs at the anodic film surface. Conversely, an increase in conductivity concentrates the electric field through the anodic film and provides particles with sufficient driving force to migrate into the bottom of the pores. Thus, the increase in the impregnation depth can be correlated with the increase in the electric field in the anodic film.

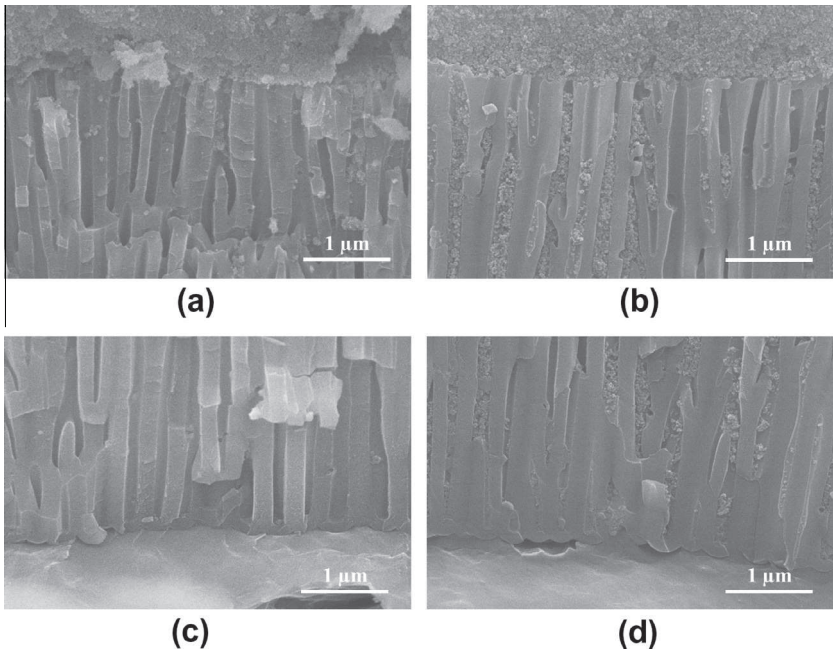

Fig. 2. FEG-SEM cross-sectional views of the porous anodic film after the EPD process using 200 V cm^{-1} for 5 min with two different suspension conductivities: 40 μS cm^{-1} (top (a) and bottom (c) of the pores) and 120 μS cm^{-1} (top (b) and bottom (d) of the pores).

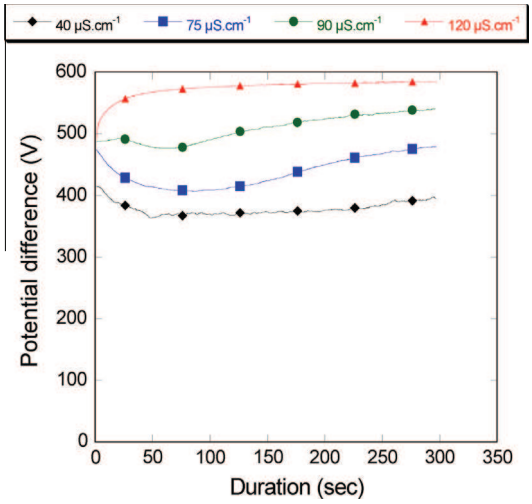

Fig. 4. Potential drop over the anodic film versus time as a function of the suspension conductivity: 45 µS cm^{-1} (♦), 75 µS cm^{-1} (■), 90 µS cm^{-1} (●), 120 µS cm^{-1} (▲).

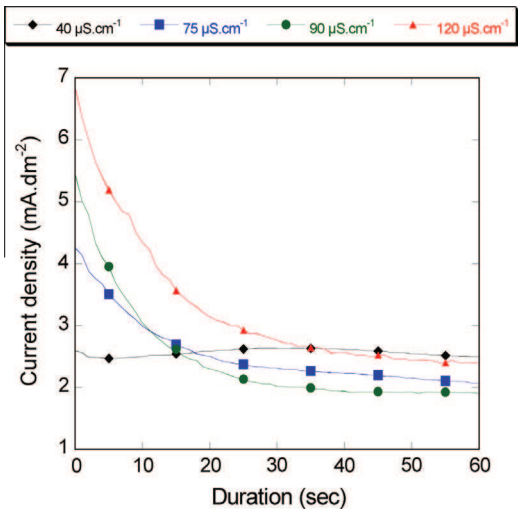

Fig. 5. Evolution of current intensity over time as a function of the suspension conductivity: 45 µS cm^{-1} (♦), 75 µS cm^{-1} (■), 90 µS cm^{-1} (●), 120 µS cm^{-1} (▲).

3.3. Study of the current density during impregnation

The current intensity was measured during electrophoretic deposition (Fig. 5). For conductivity over 40 µS cm^{-1}, the current quickly decreases before stabilising (this behaviour is often observed for electrophoretic deposits). This drop can be explained by the resistance of the deposit under formation or a particle concentration gradient in the vicinity of the deposition electrode [19]. Stabilisation would thus correspond to the end of deposition. For 40 µS cm^{-1}, the current is roughly constant meaning that the resistance due to the deposit is rather low.

The current level can be directly linked to the deposition kinetics. The initial drop was analysed using two models, considering that the time t' beyond which the drop comes to an end was graphically determined by linear extrapolation at $j = 0$. Firstly, a diffusive model, which considers that the deposition kinetics are determined by the diffusion speed of the particles towards the deposit electrode, was used. In this model, the current density $j(t)$ is directly proportional to $t^{-1/2}$ and can be described by [19]:

$$j(t) = \frac{qD^{1/2}C}{\pi^{1/2}t^{1/2}} \tag{4}$$

with $j(t)$ the current density (A m^{-2}), q the amount of electricity per mole (C mol^{-1}), D the diffusion coefficient, C the particles concentration in the suspension (mol m^{-3}) and t time (s). The current density was plotted as a function of $t^{-1/2}$ for $0 < t < t'$ (Fig. 6). The current density seems to be directly proportional to $t^{-1/2}$ only when the suspension conductivity is equal to 40 µS cm^{-1}, suggesting that the deposition kinetics are determined in this sole instance by particle diffusion.

Secondly, a resistive model was used. This model considers the EPD cell as a series of constant resistances (deposit resistance, suspension resistance and Faradic resistance at the electrode/suspension interface), except for the deposit resistance which changes and increases during its formation; the deposition kinetics are here determined by the deposit resistance and the current density can be defined by [19]:

$$j(t) = \frac{j_0}{\sqrt{1 + \frac{2j_0^2 k}{U}\left(\frac{\rho_D}{d_D}\right)t}} \tag{5}$$

with j_0 the current density at $t = 0$ (A m^{-2}), k the deposited mass/electrical charge consumed ratio (m C^{-1}), U the applied voltage (V), ρ_D the deposit resistivity (Ω m^{-1}) and d_D the deposit density (kg m^{-3}). Thus $[j_0/j(t)]^2$ is here directly proportional to time t. Fig. 7 shows that the evolution of $[j_0/j(t)]^2$ during deposition is linear when the suspension conductivity is equal to 75 µS cm^{-1}, 90 µS cm^{-1} and 120 µS cm^{-1}. This means that the initial current drop seems to be governed by the deposit resistance when conductivity is above 40 µS cm^{-1}. For low conductivity (40 µS cm^{-1}), a significant share of the potential gradient is located in the suspension. Thus, deposition can be assumed to be governed by the diffusion of particles in the suspension as the conductivity is high enough. As the diffusion of particles in the suspension no longer constitutes a limiting factor, the resistance of the deposit as it forms governs the deposition kinetics. This point is consistent with what has been already demonstrated by Stappers et al. [7]: the higher solution conductivity, the more compact deposits and thus the higher the deposit resistance.

In order to address the origin of the better impregnation obtained for higher solution conductivities, the initial resistance distribution through the cell was assessed. At $t = 0$ s, the entire resistance over the cell (R_{tot}) can be defined as the sum of the

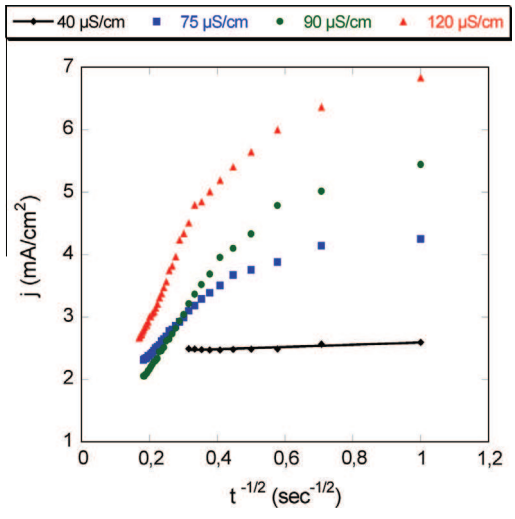

Fig. 6. $j(t)$ As a function of $t^{-1/2}$ for each suspension conductivity.

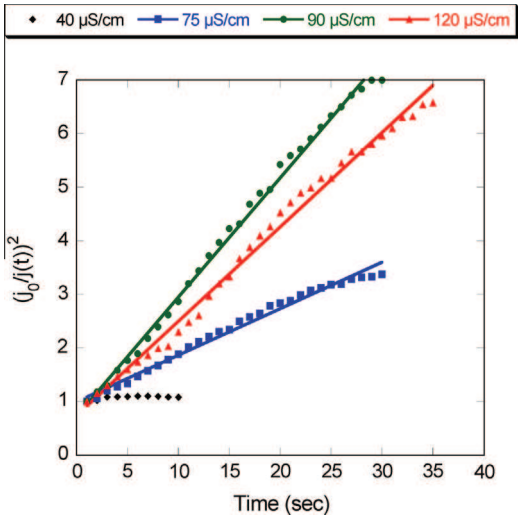

Fig. 7. $[j_0/j(t)]^2$ As a function of t for each suspension conductivity.

resistance of the suspension (R_{susp}) and the resistance of the film (R_{film}) (Fig. 8). R_{tot} can be calculated according to Ohm's law:

$$R_{tot} = \frac{U_{tot}}{I_{tot}} \tag{6}$$

with U_{tot} the voltage applied between the cathode and the anode and I_{tot} the current passing through the cathode and the anode. R_{susp} can be also calculated from the following equation:

$$R_{susp} = \frac{d}{\sigma S} \tag{7}$$

with l the length between the two electrodes, σ the suspension conductivity and S the electrode surfaces (4 cm^2). Finally R_{film} can be deduced:

$$R_{film} = R_{tot} - R_{susp} = \frac{U_{tot}}{I_{tot}} - \frac{d}{\sigma S} \tag{8}$$

These three resistances were plotted as a function of the solution conductivity (Fig. 9). It appears that R_{film} decreases as this conductivity increases. Knowing that the anodic film is made of a compact layer and a porous layer, the suspension conductivity is unlikely to have an influence on the compact layer resistivity. Nevertheless, the resistance of the porous layer is highly dependent on the suspension conductivity because of the impregnation of the suspension in the pores during immersion. At the pore wall/electrolyte interface, the ionic spatial distribution is modified due to the development of an electrical charge at the surface of the pore

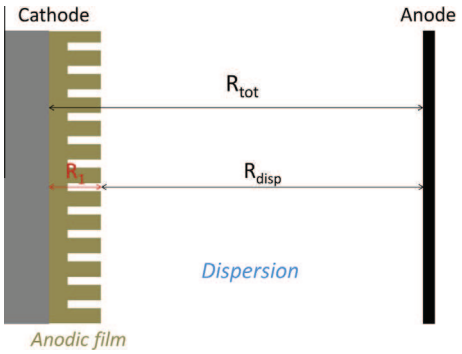

Fig. 8. Distribution of resistance between the cathode and anode before impregnation.

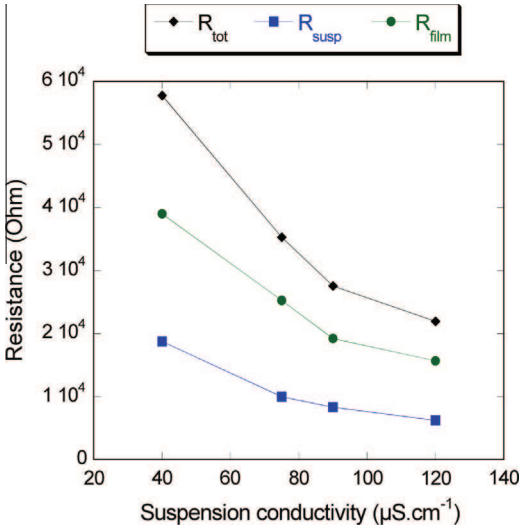

Fig. 9. Evolution of overall resistance, anodic film resistance and suspension resistance as a function of the suspension conductivity at the beginning of impregnation.

wall [20]. This leads to the formation of an electric double layer whose thickness depends on the ionic strength of the solution. The greater the conductivity, the thinner will be the double layer. Interactions between particles and the pore wall are mainly governed by the overlap of their respective double layers. For low-conductivity suspensions, the double layer can span the pores leading to reduced mass transport. Thus, the thick double layer at the pore wall/electrolyte interface will prevent migration of particles into the pores and lead to their agglomeration at the pore surface. An increase in the suspension's conductivity will reduce the thickness of the double layer that becomes compressed against the pore walls allowing for mass transport in the centre of the pores and reducing the film's resistance.

4. Conclusion

The influence of the suspension conductivity on the EPD of SiO_2 particles in a porous alumina film supported by an aluminium substrate was studied in depth. The results revealed that low-conductivity suspensions induced deposits located only at the anodic film surface, whereas high-conductivity suspensions led to particle deposition within the pores. It was shown that an increase in the suspension conductivity concentrated the electric field in the anodic film leading to an increase in the driving force of the particles to penetrate the pores. Furthermore, for low-conductivity suspensions, it can be assumed that the electric double layer at the pore/electrolyte interface had greater thickness leading to shrinkage of the effective pore diameter and therefore restricted access to the pores with an ensuing reduction in the mass of the deposit. By contrast, an increase in the suspension's conductivity compresses the electric double layer against the pores, promoting particle migration into the pores. The suspension's conductivity thus appears to be a key parameter with respect to impregnation depth.

References

[1] N. Koura, T. Tsukamoto, H. Shoji, T. Hotta, Jpn. J. Appl. Phys. 34 (1995) 1643–1647.
[2] T. Teranishi, M. Hosoe, T. Tanaka, M. Miyake, J. Phys. Chem. B 103 (1999) 2318–3827.
[3] A.R. Boccaccini, J. Cho, J.A. Roether, B.J.C. Thomas, E.J. Minay, M.S.P. Shaffer, Carbon 44 (2006) 3149–3160.
[4] J. Escobar, L. Arurault, V. Turq, Appl. Surf. Sci. 258 (2012) 8199–8208.

[5] L. Bazin, M. Gressier, P.L. Taberna, M.J. Menu, P. Simon, Chem. Commun. (2008) 5004–5006.
[6] L. Besra, M. Liu, Prog. Mater. Sci. 52 (2007) 1–61.
[7] L. Stappers, L. Zhang, O. Van der Biest, J. Fransaer, J. Colloid Interface Sci. 328 (2008) 436–446.
[8] B. Ferrari, R. Moreno, J. Eur. Ceram. Soc. 17 (1997) 549–556.
[9] K. Hasegawa, S. Kunugi, M. Tatsumisago, T. Minami, J. Sol–Gel Sci. Technol. 15 (1999) 243–249.
[10] S. Dor, S. Rühle, A. Ofir, M. Adler, L. Grinis, A. Zaban, Colloid Surf. A: Physicochem. Eng. Asp. 342 (2009) 70–75.
[11] S.J. Limmer, S. Seraji, Y. Wu, T. Chou, C. Nguyen, G. Cao, Adv. Funct. Mater. 12 (2002) 59–64.
[12] K. Kamada, H. Fukuda, K. Maehara, Y. Yoshida, M. Nakai, S. Hasuo, Y. Matsumoto, Electrochem. Solid-State Lett. 7 (2004) B25–B28.
[13] B. Fori, P.L. Taberna, L. Arurault, J.P. Bonino, C. Gazeau, P. Bares, Colloid Surf. A: Physicochem. Eng. Asp. 415 (2012) 187–194.
[14] S.J. Limmer, T.P. Chou, G.Z. Cao, J. Sol–Gel Sci. Technol. 36 (2005) 183–195.
[15] S. Cousinié, M. Gressier, P. Alphonse, M.J. Menu, Chem. Mater. 19 (2007) 6492–6503.
[16] L. Dusoulier, R. Cloots, B. Vertruyen, R. Moreno, O. Burgos-Montes, B. Ferrari, J. Eur. Ceram. Soc. 31 (2011) 1075–1086.
[17] K. Kamada, M. Mukai, Y. Matsumoto, Mater. Lett. 57 (2003) 2348–2351.
[18] L. Arurault, G. Zamora, V. Vilar, P. Winterton, R. Bes, J. Mater. Sci. 45 (2010) 2611–2618.
[19] C. Baldisserri, D. Gardini, C. Galassi, J. Colloid Interface Sci. 347 (2010) 102–111.
[20] G. Anné, B. Neirinck, K. Vanmeensel, O. Van der Biest, J. Vleugels, J. Am. Ceram. Soc. 89 (2006) 823–828.